Journal of Sound and Vibration (2002) **252**(3), 563–572
doi:10.1006/jsvi.2001.4051, available online at http://www.idealibrary.com on IDEAL®

QUALITATIVE AND QUANTITATIVE ANALYSIS OF STOCHASTIC PROCESSES BASED ON MEASURED DATA, II: APPLICATIONS TO EXPERIMENTAL DATA

J. GRADIŠEK, E. GOVEKAR AND I. GRABEC

Faculty of Mechanical Engineering, University of Ljubljana, Aškerčeva 6, SI-1000 Ljubljana, Slovenia.
E-mail: janez.gradisek@fs.uni-lj.si

(*Received* 30 *April* 2001, *and in final form* 1 *August* 2001)

Analysis of stochastic processes governed by the Langevin equation is discussed. The analysis is based on a general method for non-parametric estimation of deterministic and random terms of the Langevin equation directly from given data. Separate estimation of the terms corresponds to the decomposition of process dynamics into deterministic and random components. Part I of the paper presented several possibilities for qualitative and quantitative analysis of process dynamics based on such decomposition. In Part II, some of these analysis possibilities are applied to experimental datasets from metal cutting and laser-beam welding.

1. INTRODUCTION

Most experimental data are to some extent noisy. Data can be noisy due to either the measurement procedure or the process generating the data. In the former case, the noise is superimposed on the measured data and uncorrelated to the process dynamics, while in the latter case the noise represents a constitutive part of the process dynamics, and the process is therefore stochastic. In Part I of this paper [1], analysis of stochastic processes with uncorrelated Gaussian noise was discussed. Such processes can be modelled by the Langevin equation, in which the temporal evolution of a process is determined by a sum of deterministic and random terms. The deterministic term usually describes the global dynamics of the process, whereas the random term describes some kind of environmental noise or noisy input which affects the process state but does not affect the process parameters. It was shown in Part I [1] as to how both the deterministic and random terms can be estimated from data and analyzed. The aim here is to apply these analysis methods to analyze experimental data from metal cutting and laser-beam welding. Metal cutting is an example in which the deterministic and random terms of the Langevin equation can be related quite reasonably to the actual physical phenomena involved in the process. For laser-beam welding, such relations are not easy to establish. However, the analysis methods presented in reference [1] can nevertheless be used to extract relevant information about the process dynamics from stochastic data.

2. ANALYSIS OF EXPERIMENTAL DATA

2.1. METAL CUTTING

The dynamics of metal cutting involve various non-linear phenomena such as material flow and fracture, friction between the tool and the workpiece, coupled vibrations of

0022-460X/02/$35.00

a machine–tool–workpiece structure, etc. When a cutting process is modelled on a macroscopic scale as a mechanical oscillatory system, the dynamics of the cut material can be treated as a source of random influence on a deterministic process. Assuming that these influences are uncorrelated and Gaussian, the dynamics of metal cutting can be modelled by the Langevin equation in which the deterministic and random terms describe the deterministic machine–tool–workpiece dynamics and the random influences of the cut material respectively.

In machining literature, two dynamically different cutting regimes are roughly distinguished: chatter-free cutting and cutting accompanied by chatter. Chatter denotes self-excited large-amplitude vibration of the machine–tool–workpiece structure. As an unfavorable cutting regime, chatter has been studied intensively. Analyses of non-linear models of a cutting process have revealed that the transition from chatter-free cutting to chatter corresponds to a sub-critical Hopf bifurcation from a stable fixed point to a stable limit cycle [2, 3]. These analytical results have been confirmed experimentally [4]. As shown in reference [5] and below, evidence in favor of such a description of chatter onset can also be obtained by time-series analysis using the methods discussed in reference [1].

As an example of a cutting process, turning on a lathe was chosen where a rotating workpiece is cut by a fixed tool. The experimental set-up is illustrated schematically in Figure 1. A dynamometer was used to measure fluctuations of the cutting force **F**. The signals were sampled at a frequency of 100 kHz and each contained 220 000 data points. Details of the experiments can be found elsewhere [5].

Chatter-free and chatter-cutting regimes were achieved by varying the cutting depth a while keeping the rest of the cutting parameters constant. Portions of the cutting force fluctuations recorded in the two cutting regimes are shown in Figure 2. In the chatter-free regime, the cutting force F_c fluctuated erratically with occasional bursts of high-frequency periodic oscillations (Figure 2(a)), whereas in the chatter regime pronounced periodic fluctuations of the cutting force were observed with a dominant frequency markedly lower than in the chatter-free regime (Figure 2(b)).

The deterministic and random components of cutting dynamics, **h** and **G**, were estimated in a two-dimensional phase space reconstructed from the recorded time series of the cutting component F_c of **F** using the delay co-ordinates, $\mathbf{x}(t) = (F_c(t - \tau), F_c(t))$. The delay τ was chosen as the time where the autocorrelation function decays to $1/e$, as suggested in

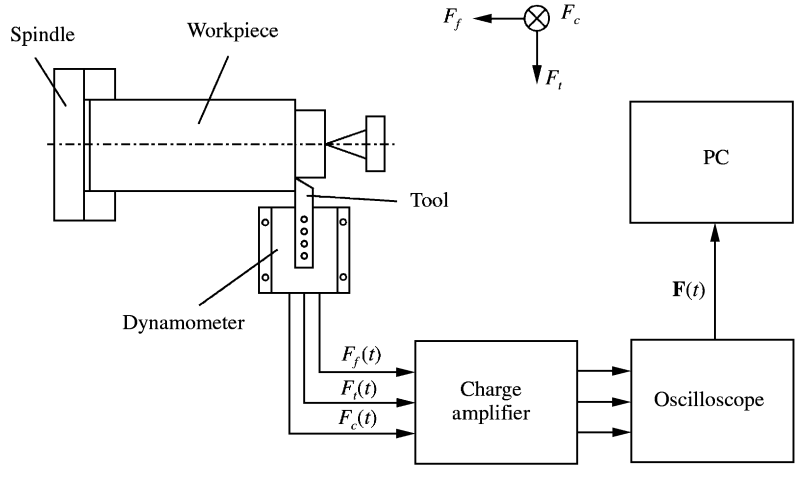

Figure 1. Experimental set-up for turning.

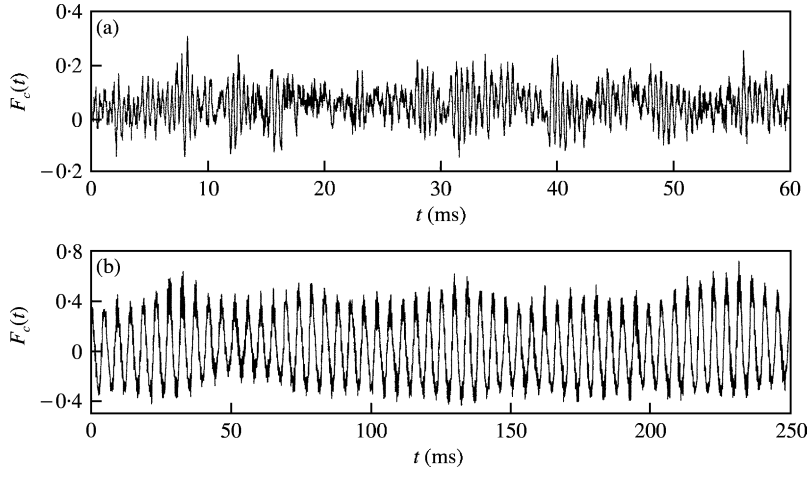

Figure 2. Portions of the recorded cutting force fluctuations: (a) chatter-free regime, $a = 0{\cdot}3$ mm; (b) chatter regime, $a = 1$ mm. Note the difference in the scales of the two figures.

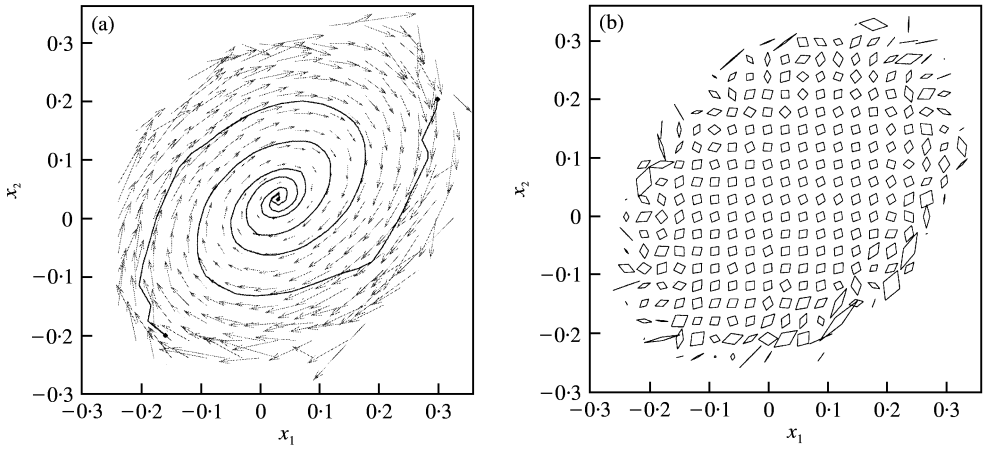

Figure 3. Estimated terms **h** and **G** in the chatter-free cutting regime: (a) deterministic term **h** shown as a vector field with two reconstructed deterministic trajectories superimposed; (b) random term **G** shown as a field of parallelograms. $\mathbf{x}(t) = (F_c(t - 0{\cdot}1\,\text{ms}),\ F_c(t))$.

reference [6]. In the chatter-free regime, arrows in the vector field of **h** point on average in the clockwise direction and indicate spiralling motion towards a stable fixed point located close to the center of the phase space (Figure 3(a)). Both reconstructed deterministic trajectories superimposed on the field start from the edge of the phase portrait, follow spiral paths, and terminate at a fixed point. Stability analysis of the fixed point based on approximation of **h** by a third order polynomial yields eigenvalues of the Jacobian matrix $s_{1,2} \approx -2{\cdot}6 \pm 11\text{i}$, which confirm that the fixed point is a stable focus. Cutting force fluctuations in chatter-free cutting can therefore be described as random fluctuations around a stable fixed point. Parallelograms in the field of **G** have a similar size and orientation across the entire phase space (Figure 3(b)), indicating constant amplitude of noise. Parallelograms at the edge of the phase space have different shapes and sizes, presumably because of the statistically poor estimate of **G** in that region.

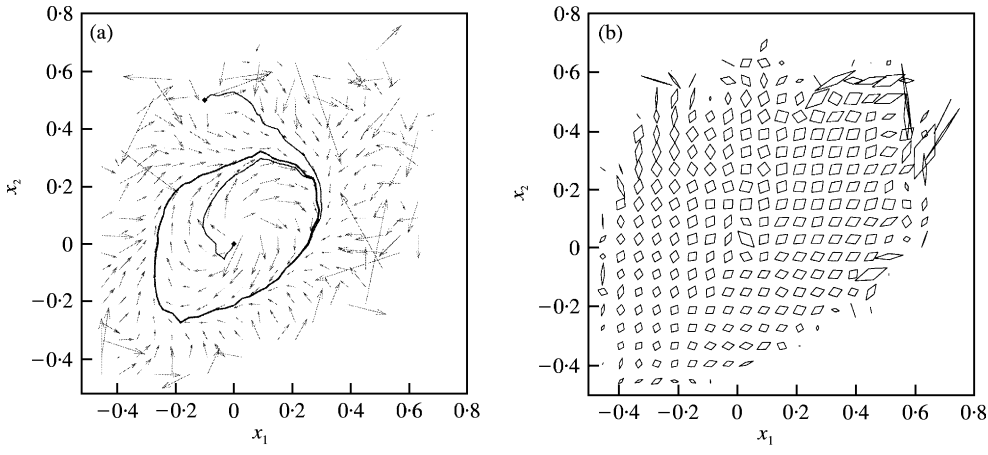

Figure 4. Estimated **h** and **G** in the chatter-cutting regime. (a) Deterministic term **h** shown as a vector field with two reconstructed deterministic trajectories superimposed; (b) random term **G** shown as a field of parallelograms. $\mathbf{x}(t) = (F_c(t - 0{\cdot}85\,\text{ms}),\ F_c(t))$.

In the chatter regime, arrows in the vector field of **h** indicate motion on a stable non-symmetric limit cycle (Figure 4(a)). The reconstructed trajectories superimposed on the field start from the center and the edge of the phase portrait, respectively, and both terminate in a limit cycle. These results suggest that cutting force fluctuations in the chatter regime can be described as random fluctuations around a stable limit cycle.

Furthermore, the path of the trajectory starting from the center of the phase space and the arrows inside the limit cycle also reveal that an unstable fixed point might be located in the vicinity of the center. Using a third order polynomial approximation of **h**, eigenvalues $s_{1,2} \approx 0{\cdot}2 \pm 1{\cdot}7\text{i}$ are obtained at the fixed point, which confirms that it is unstable. More detailed inspection of the field of **h** reveals that arrows in the left region of the phase space are aligned almost in parallel to the limit cycle, indicating low local dissipation. In the opposite region of the phase portrait, and arrows are inclined strongly towards the limit cycle, an indication of high local dissipation. These two portions of the limit cycle correspond to the tool motion away from and towards the workpiece respectively. Different local dissipations in these two regions presumably result from the dependence of damping on the relative direction of the tool motion with respect to the workpiece. Parallelograms in the field of **G** differ in size and shape according to the location in phase space (Figure 4(b)). Large parallelograms are found in the upper right region of the phase portrait corresponding to the instants of minimum contact between the tool and the workpiece. Small parallelograms occupy the lower left region of the phase portrait which corresponds to the instants of maximal penetration of the tool into the workpiece. Between these two regions, the average orientation of parallelograms in **G** changes from horizontal to vertical and *vice versa.*

Comparison of the estimated deterministic terms of the two cutting regimes shows that a transition from the chatter-free to the chatter regime in fact represents a transition from a stable fixed-point attractor to a stable limit-cycle attractor with an embedded unstable fixed point. Such a change of attractors is indeed typical of the Hopf bifurcation [7].

When analyzing experimental data, the correct forms of the deterministic and random terms are usually not known. One way to examine the validity of the estimated **h** and **G** is to verify their convergence as time step τ in the conditional moments is decreased [1]. For the chatter-cutting regime, the dependence of components of **h** and **G** on the time step τ is

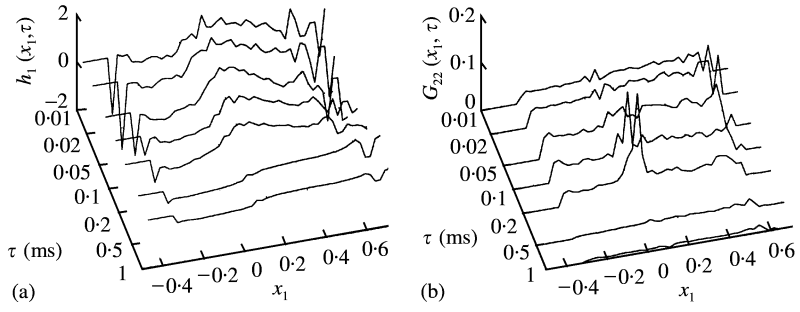

Figure 5. Dependence of estimated terms in chatter regime on time step τ. Cross-sections of the terms at $x_2 \approx 0{\cdot}1$ are shown: (a) component of the deterministic term **h**; (b) component of the random term **G**. $\mathbf{x}(t) = (F_c(t - 0{\cdot}85\,\text{ms}),\ F_c(t))$.

illustrated in Figure 5. The estimates of the deterministic term **h** remain relatively unchanged for $\tau \leqslant 0{\cdot}2$ ms (Figure 5(a)), which means that $\tau \leqslant 0{\cdot}2$ ms is the maximum time step providing a reliable estimate of **h**. Estimates of the random term **G** have on average a similar shape for $\tau \leqslant 0{\cdot}05$ ms (Figure 5(b)), but their value changes as τ is further decreased. The lack of convergence of the random term indicates that the noise may not be uncorrelated as assumed in the Langevin equation. Similar results are obtained for the chatter-free regime (not shown), except that the maximum acceptable time step for the estimation of **h** is $\tau = 0{\cdot}1$ ms.

2.2. LASER-BEAM WELDING

Laser-beam welding is a joining technique in which the components to be joined are locally melted by a laser beam. The physical phenomena taking place in the pool of molten material, such as heat conduction, melting, evaporation, and solidification of material, fluid flow, generation of plasma, etc., determine the dynamics of laser-beam welding [8, 9]. By varying the power density supplied to the workpiece by the laser beam, various welding regimes can be achieved. In the present study, two regimes of CO_2-laser-beam welding are considered: deep and shallow-penetration welding. High power densities are required for deep-penetration welding. The energy supplied to the workpiece causes intense vaporization of the material, such that a capillary known as a keyhole is created in the molten pool [8, 9]. The keyhole enables deeper penetration of the laser beam into the material, which deepens the molten pool. Shallow-penetration welding occurs at lower power densities, where the material vaporization is less intense and no keyhole is formed. The penetration depth of the laser beam is therefore considerably smaller, and the molten pool shallower.

Although both welding regimes are technologically useful, deep penetration welding has mainly been studied [8–10]. However, comparison of analytical and experimental results is hindered by experimental difficulties involved in measurements of the physical quantities meaningfully related to process dynamics. The most common measurement is of fluctuations in the intensity of light emitted by the welding process at a certain wavelength [10, 11]. The recorded signals are usually noisy, and severe filtering has been suggested to make them suitable for analysis by methods of deterministic chaos [10]. Experimental analysis of welding dynamics is also motivated by the need for reliable monitoring of the process. One example of a monitoring task of practical relevance is the detection of a transition from deep- to shallow-penetration welding [11].

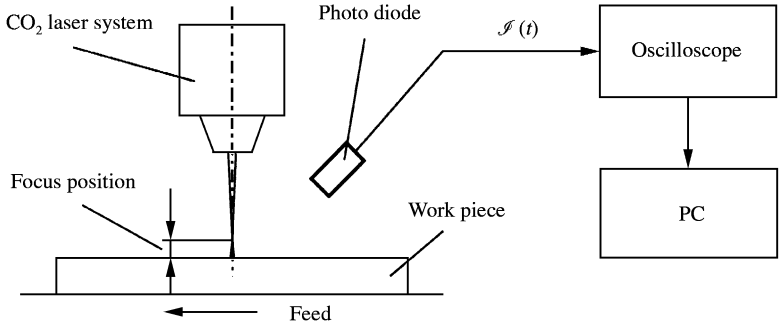

Figure 6. Experimental set-up for CO_2-laser-beam welding.

Our aim here is to use the methods presented in reference [1] to analyze the light intensity fluctuations recorded in the two welding regimes. Due to the multitude and complex interplay of physical phenomena occurring in laser-beam welding, the relationships between the phenomena and the terms of the Langevin equation are difficult to establish. Nevertheless, it is shown below that such an analysis can shed some light on the physical properties of the laser-welding by dynamics, as well as provide a possible solution of the aforementioned monitoring task.

The experimental set-up for the CO_2-laser-beam welding of steel workpieces is shown schematically in Figure 6. A photo diode was used to detect fluctuations of light intensity $\mathscr{I}$ emitted by the welding process at a wavelength of 540 ± 10 nm. The signals were sampled at a frequency of 45 kHz and each contained 180 000 data points. Details about the experiments can be found in reference [12].

Deep- and shallow-penetration welding regimes were achieved by varying the focus position f_L of the laser beam while keeping other process parameters constant. Portions of the light intensity fluctuations recorded in the two welding regimes are shown in Figure 7. In deep-penetration welding, irregular, random-like fluctuations of light intensity $\mathscr{I}$ were observed (Figure 7(a)). The occasional dramatic increases of $\mathscr{I}$ followed by significant drops presumably correspond to the keyhole activity and plasma effects in the molten pool. These spiky patterns skew the amplitude distribution of the intensity fluctuations (not shown). In shallow-penetration welding, irregular fluctuations of light intensity are interspersed with short segments of distinct periodic oscillations (Figure 7(b)). Events related to the keyhole activity cannot be observed.

The deterministic and random components of laser-beam welding dynamics, **h** and **G**, were estimated in a two-dimensional phase space reconstructed from the recorded time series of light intensity fluctuations using the delay coordinates [6], $\mathbf{x}(t) = (\mathscr{I}(t-\tau), \mathscr{I}(t))$. Again, the delay τ was chosen as the time where the autocorrelation function decays to $1/e$. In deep-penetration welding, the arrows in **h** point on average towards a fixed point at $\mathbf{x} \approx (0{\cdot}5, 0{\cdot}5)$ (Figure 8(a)). The reconstructed deterministic trajectories superimposed on the field all start at the edge of the phase portrait and, without spiralling, terminate at this fixed point. Using a third order polynomial approximation of **h**, the fixed point is found to be a stable node, $s_1 \approx -2{\cdot}5$ and $s_2 \approx -4{\cdot}6$. One concludes that the light intensity fluctuations in the deep-penetration welding regime can be described as random fluctuations around a stable node.

Parallelograms in the field of **G** differ significantly in size, indicating that noise amplitude is not constant across the phase portrait. Disregarding the parallelograms at the edge of the phase portrait, the noise amplitude increases with the distance from the lower left corner of

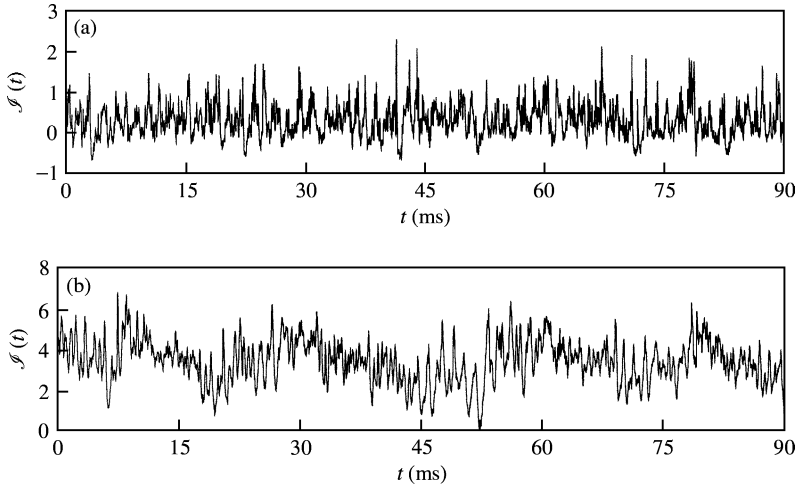

Figure 7. Portions of light intensity time series: (a) deep penetration welding regime, $f_L = 0{\cdot}5\,\text{mm}$ above the workpiece surface; (b) shallow-penetration welding regime, $f_L = 2\,\text{mm}$.

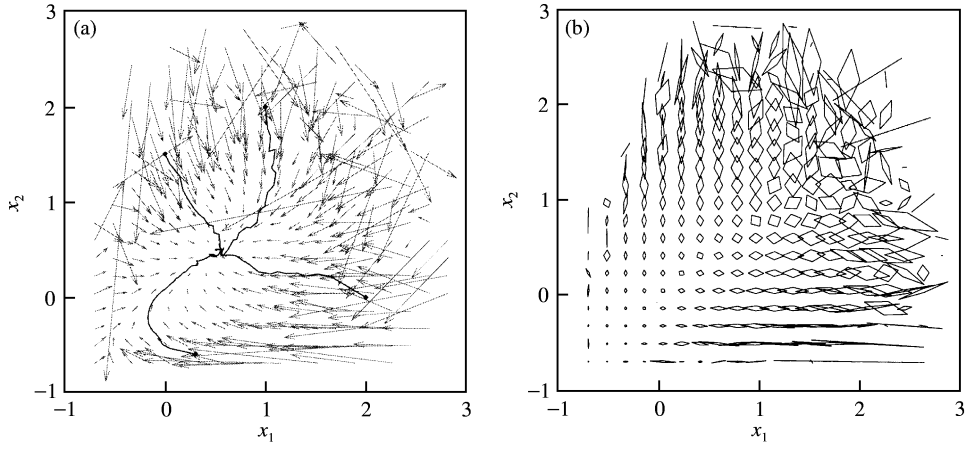

Figure 8. Estimated terms **h** and **G** in the deep-penetration welding regime: (a) deterministic term **h** shown as a vector field with four reconstructed deterministic trajectories superimposed; (b) random term **G** shown as a field of parallelograms. $\mathbf{x}(t) = (\mathscr{I}(t - 0{\cdot}16\,\text{ms}), \mathscr{I}(t))$.

the phase portrait. Such a distribution of the estimated noise amplitude can be explained by slower and smaller changes of the trajectory path in the region of small light intensity. The parallelograms on the right and the left region of the phase portrait are oriented horizontally and vertically respectively. These two regions are mainly visited by the process trajectory during the distinct spiky patterns related to the keyhole and plasma activities, when the trajectory makes rather large leaps per sampling interval.

In shallow-penetration welding, arrows in the vector field of **h** point on average in the clockwise direction and indicate spiralling towards a fixed point located at $\mathbf{x} \approx (3{\cdot}6,\ 3{\cdot}3)$ (Figure 9(a)). Indeed, the reconstructed trajectories starting at the edge of the phase portrait both follow a spiral path terminating in the fixed point. Stability analysis of the fixed point using a third order polynomial approximation of **h** yields $s_{1,2} \approx -0{\cdot}45 \pm 2{\cdot}1\text{i}$. This means that light intensity fluctuations in shallow-penetration welding can be described as random fluctuations around a stable focus.

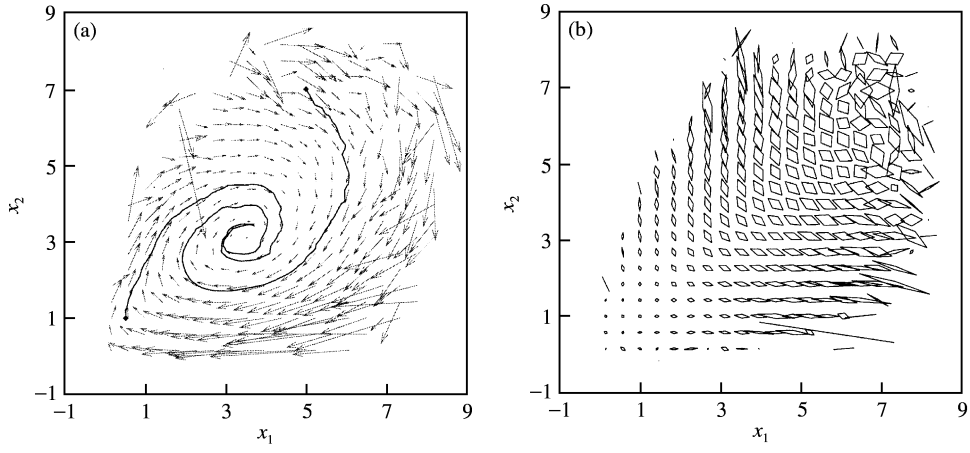

Figure 9. Estimated terms **h** and **G** in the shallow-penetration welding regime. (a) Deterministic term **h** shown as a vector field with two reconstructed deterministic trajectories superimposed; (b) random term **G** shown as a field of parallelograms. $\mathbf{x}(t) = (\mathscr{I}(t - 0{\cdot}29\,\text{ms}), \mathscr{I}(t))$.

The distribution of noise amplitude (Figure 9(b)) is similar to that of the deep-penetration welding (Figure 8(b)). Notable differences are observed in the upper right corner, and in the left and the right regions of the phase portrait. These differences can mainly be attributed to the absence of the distinct spiky patterns in the light intensity fluctuations of shallow-penetration welding (Figure 7).

Comparison of the estimated deterministic terms of deep and shallow-penetration welding reveals that a transition between the two welding regimes manifests itself as a change in the nature of the attracting fixed point. Monitoring of the eigenvalues of the Jacobian matrix $s_{1,2}$ evaluated at the fixed point therefore provides the information needed to detect this transition.

To conclude the analysis of laser-beam welding dynamics, the convergence of the estimated **h** and **G** is examined as time step τ in the conditional moments is decreased. In Figure 10, the dependences $\mathbf{h}(\tau)$ and $\mathbf{G}(\tau)$ are shown for deep-penetration welding. Both the deterministic **h** and random term **G** reach the final shape at $\tau = 0{\cdot}044$ ms. The value of **h** also remains similar for $\tau = 0{\cdot}022$ ms, whereas the value of **G** changes. These results give more confidence in the estimate of **h** than in that of **G**. However, the short τ interval of relatively constant **h** indicates that the sampling rate of the light intensity fluctuations should be increased to enable more reliable estimates of **h** and **G**. Similar conclusions are reached for shallow-penetration welding (not shown).

3. DISCUSSION AND CONCLUSIONS

This paper discusses the possibilities for qualitative and quantitative analysis of stochastic processes based on measured data. In the first part of the paper, the analysis possibilities were presented and illustrated using synthetic datasets. In this part of the paper, the methods were applied to experimental datasets from two regimes of turning and CO_2-laser-beam welding. In the turning example, the chatter-free and the chatter-cutting regime were analyzed based on the recorded fluctuations of the cutting force. It was found that the dynamics of the two regimes can be described as random fluctuations around a stable fixed point and a stable limit cycle respectively. These results support the

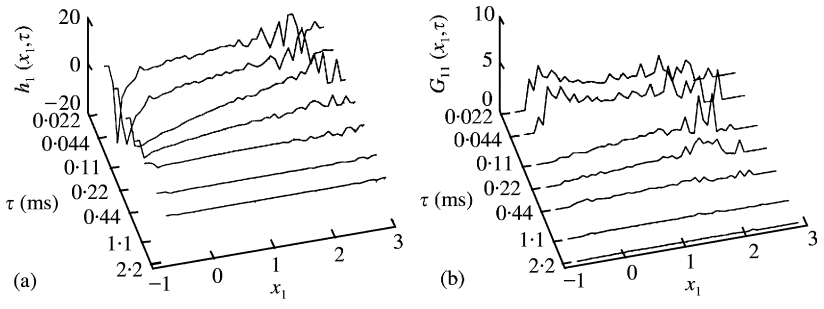

Figure 10. Dependence of estimated terms in deep-penetration welding on the time step τ. A cross-section of the terms at $x_2 \approx 1$ is shown. (a) Component of the deterministic term **h**; (b) component of the random term **G**. $\mathbf{x}(t) = (\mathscr{I}(t - 0{\cdot}16\,\text{ms}), \mathscr{I}(t))$.

description of chatter onset as a Hopf bifurcation. In the CO_2-laser-beam welding example, deep- and shallow-penetration welding regimes were analyzed based on the recordings of the light intensity fluctuations emitted by the welding process. The dynamics of the two regimes were described as random fluctuations around a stable fixed point. In deep-penetration welding the fixed point was a node, whereas in shallow-penetration welding it was a focus. It was suggested that such a distinction between the dynamics of the two regimes could be exploited to detect a transition between the two welding regimes.

Both processes were analyzed in a two-dimensional phase space reconstructed from a measured scalar variable. The reasons for restricting the analyses to two dimensions are the following. Various non-linear deterministic models of metal cutting on a macroscopic scale suggest that cutting dynamics evolve on a low-dimensional attractor [2–4, 13], although phase spaces of these models have four, or even infinitely many, dimensions. The experimental data have also been analyzed in a three-dimensional reconstructed space [5], and the results obtained are equivalent to those quoted above. The situation is different in the case of laser-beam welding, where very little information is available about the original phase space, the underlying deterministic attractor, their properties and dimensions. The relation between the measured physical quantity and the process dynamics is also not clear. It, therefore, seems reasonable to analyze data in a low-dimensional space before extending the analysis to higher dimensions. In the present case, analysis of data in two- and three-dimensional reconstructed spaces yielded similar results.

When there are indications that the process under inspection is chaotic, the reconstructed phase space should certainly span more than two dimensions. In order to verify whether the phase space dimension is sufficiently large, one should compare the reconstructed deterministic trajectories rather than the vector fields or their cross-sections. Once the sufficient phase space dimension has been chosen, the trajectories will not change significantly as the dimension is further increased. In the case of the stochastic Lorenz system in a chaotic regime analyzed in Part I of this paper [1], the reconstructed deterministic trajectories visit both lobes of the attractor interchangeably only if the reconstructed phase space is at least three-dimensional.

The analysis methods presented in this paper are applicable in principle only to stochastic processes which can be described by the Langevin equation. These processes contain uncorrelated dynamic noise which does not affect the process parameters. The metal-cutting process, for example, can be modelled as a mechanical oscillatory system influenced by the flow of the non-homogeneous cut material. Other mechanical systems which can be modelled analogously include: an airplane wing influenced by the airflow [14, 15], a vehicle system influenced by road conditions, etc. However, analysis of processes

for which the relations between the physical phenomena and the terms of the Langevin equation cannot be reliably established, may also yield information relevant for both modelling and monitoring purposes. This shows that the methods are applicable to analysis of stochastic data, especially when noisiness of the data cannot be neglected.

ACKNOWLEDGMENTS

The authors thank Prof Manfred Geiger and his collaborators for their cooperation with the laser-beam welding experiments which were conducted at the Chair of Manufacturing Technology, University of Erlangen, Germany. The authors acknowledge the support of the Volkswagen Foundation, the Ministry of Education and Science of Slovenia, and the EU COST Action P4. EG also thanks the Alexander von Humboldt Foundation for their support.

REFERENCES

1. J. GRADIŠEK, S. SIEGERT, R. FRIEDRICH and I. GRABEC 2002 *Journal of Sound and Vibration* **252**, 545–562. Qualitative and quantitative analysis of stochastic processes based on measured data—I. Theory and applications to synthetic data.
2. A. H. NAYFEH, C.-M. CHIN and J. R. PRATT 1997 *American Society of Mechanical Engineers Journal of Manufacturing Science and Engineering* **119**, 485–493. Perturbation methods in nonlinear dynamics—applications to machining dynamics.
3. J. GRADIŠEK, E. GOVEKAR and I. GRABEC 2001 *Journal of Sound and Vibration* **242**, 829–838. Chatter onset in non-regenerative cutting: a numerical study.
4. T. KALMÁR-NAGY, J. R. PRATT, M. A. DAVIES and M. D. KENNEDY 1999 *Proceedings of the* 17*th American Society of Mechanical Engineers Biennial Conference on Mechanical Vibration and Noise*, 1999 *American Society of Mechanical Engineers Design and Technical Conferences*, 1–9 Las Vegas, Nevada. Experimental and analytical investigation of the subcritical instability in metal cutting.
5. J. GRADIŠEK, S. SIEGERT, R. FRIEDRICH and I. GRABEC 2001 *Mechanical Systems and Signal Processing*, to appear. Stochastic dynamics of metal cutting: bifurcation phenomena in turning.
6. H. KANTZ and T. SCHREIBER 1997 *Nonlinear Time Series Analysis*, Vol. 7, Cambridge Nonlinear Science Series, Cambridge: Cambridge University Press.
7. S. H. STROGATZ 1994 *Nonlinear Dynamics and Chaos*. Reading MA: Addison–Wesley.
8. C. TIX and G. SIMON 1994 *Physical Review* E **50**, 453–462. Model of a laser heated plasma interacting with walls arising in laser keyhole welding.
9. T. KLEIN, M. VICANEK, J. KROOS, I. DECKER and G. SIMON 1994 *Journal of Physics D*: *Applied Physics* **27**, 2023–2030. Oscillations of the keyhole in penetration laser beam welding.
10. J. KURZYNA 1998 *Journal of Physics D*: *Applied Physics* **31**, 680–692. Seraching for chaos in fluctuations of a plasma induced during cw–CO_2 laser welding.
11. S. NAKAMURA, M. SAKURAI, K. KAMIMUKI, T. INOUE and Y. ITO 2000 *Journal of Physics D*: *Applied Physics* **33**, 2941–2948. Detection technique for transition between deep penetration mode and shallow penetration mode in CO_2 laser welding of metals.
12. E. GOVEKAR, J. GRADIŠEK, I. GRABEC, M. GEISEL, A. OTTO and M. GEIGER 2000 *Untersuchung Nichtlinear-Dynamischer Effekte in Produktionstechnischen Systemen* (B. Scholz-Reiter editor), 3. Symposium der Volkswagen Stiftung Cottbus, Germany. On characterisation of CO_2 laser welding process by means of light emitted by plasma and images of weld pool.
13. I. GRABEC 1986 *Physics Letters* **117**, 384–386. Chaos generated by the cutting process.
14. M. G. GOMAN, G. I. ZAGANOV and A. V. KHRAMTSOVSKY 1997 *Progress in Aerospace Sciences* **33**, 539–586. Application of bifurcation methods to nonlinear flight dynamics problems.
15. L. E. CHRISTIANSEN, T. LEHN-SCHIØLER, E. MOSEKILDE, P. GRANASY and H. MATSUSHITA 2002 *Mathematics and Computers in Simulation* **58**, 385–405. To appear. Nonlinear characteristics of randomly excited transonic flutter.